J. Eur. Opt. Society-Rapid Publ. 2023, **19**, 5

https://doi.org/10.1051/jeos/2023003
Available online at: https://jeos.edpsciences.org

Journal of the European Optical Society-Rapid Publications

RESEARCH ARTICLE

OPEN ACCESS

An attempt to apply laser combustion to palm waste

Fatima M. Awad[1], Yousef A. Alsabah[2], Ali A.S. Marouf[3,*], and Mohammed U. Orsod[3]

[1] Department of Physics, College of Science, Sudan University of Science and Technology, P.O. Box 407, 11113 Khartoum, Sudan
[2] Department of Physics, Faculty of Education and Applied Science, Hajjah University, Hajjah, Yemen
[3] Institute of Laser, Sudan University of Science and Technology, P.O. Box: 407, 11113 Khartoum, Sudan

Received: 17 September 2022 / Accepted: 10 January 2023

Abstract. The focus of this study was to develop a method to demonstrate the feasibility of obtaining useful and high-value resources from *Phoenix dactylifera* residues and, to determine the physical and chemical properties of the ash of dates-palm-tree remains. Date-palm leaves and fiber samples were combusted for 50 s, using an Nd: YAG laser with 40 W output power. It was found, that combustion of one gram of agricultural waste could be completed in 50 s and 40 W by laser while 10 g required 1.5–10 min and 300–800 W power by microwave and at least 2 h with 1500 W power for conventional heating for 10 g. The subjects of this treatment, the leaves and fiber samples, before and after combustion were investigated by X-Ray Diffraction (XRD) and Fourier Transform Infrared (FTIR). The XRD results of the palm-fiber after combustion reveal that the samples were crystallized with a rhombohedral phase of acetamide and hatrurite, orthorhombic finite, and $Ca_4Si_2O_6(CO_3)(OH)_2$, and a monoclinic phase of ikaite properties. The XRD patterns of palm-leaf after combustion reveal that the samples were crystallized with orthorhombic hillebrandite, rhombohedral acetamide, and the monoclinic phase of each karpatite, morganite, and howlite. Finally, the FTIR exhibited several absorbance peaks, assigned to silica.

Keywords: Agriculture waste combustion, Date palm tree residues, Laser-based combustion, Laser-matter interaction, Waste utilization.

1 Introduction

Date palm (*Phoenixdactylifera*) leaves, called fronds, are pinnate, compound leaves spirally arranged around the trunk. The fully mature leaf is 4 m long, but ranges from 3 to 6 m, and is 0.5 m wide at the middle midrib that narrows toward both leaf ends. Date-palm tree residues are one of the most significant natural fibers, obtained by the annual palm trees pruning as an agricultural practice. Worldwide, there are approximately 105 million palm trees, and it is estimated that more than 3,675,000 tons of residue are produced seasonally [1]. As these agricultural and horticultural residues are plentiful, widespread and easily accessible, researchers are currently studying their application as raw-material substitutes [2]. Several burning approaches are used to convert the agricultural waste into useful value-added products, which could decrease the cost of waste disposal. There are challenges of using conventional heating vis-a-vis the laser-based combustion. Recently, Gawbah *et al.* (2018) reported the preparation of silica and silicon carbide from wheat roughage and sesame seed cake by Nd: YAG laser as the combustion source [3, 4]. In addition, rice husk ash, which is rich in silica (92–97%), can be an economically feasible raw material to produce silica gel and powders [5]. Date palm fibers have high cellulose and low lignin content which ensures good mechanical strength; hence, used for making bricks with good thermal characteristics [6], and for producing medium density fiberboard [7].

Laser techniques are being utilized in combustion control and diagnostics [8]. The thermodynamic requirements of a high-compression ratio and high-power density are well fulfilled by laser ignition [9], which can promote the combustion operation and reduce pollutant fashioning [10]. Lasers have appropriate high-power with low divergence for focusing down to the desired size with enough power density to burn samples at high pressure. Lasers with high-power and beam pointing stabilities are fundamental for producing a heating spot at a constant temperature in a fixed position [11].

In general, ceramics are known as polymorphs, with the same type of chemistry but various crystalline structures. Traditionally, ceramics are classified as clay-based materials, and can be known as inorganic and non-metallic matters that are heat treated during processing or use. They tend to be crisp, hard and inert, with ionic or covalent

* Corresponding author: marouf.44@gmail.com

bonding. Portlander is a beneficial prototype for hydrous and cement at high pressure because of its structural and chemical simplicity [12]. These materials produced from the organic materials (agricultural waste) which we treated by the method that we utilized. In this paper, we focus on utilization of laser technology to convert agricultural waste into a useful value-added product; particularly, date-palm-tree residues in producing minerals, portlandite, graphite, which could decrease the cost of waste disposal in the same time.

2 Materials and methods

2.1 Experimental

Date-palm-tree leaves and fibers samples were collected from the institutional garden of Sudan University of Science and Technology in Khartoum, Sudan. Samples were washed with distilled water to clean off stucked soil, debris and other contaminants, and air-dried at room temperature. Dried samples were then ground into powder by using a mortar and pestle. One gram of each sample was placed in a crucible and combusted the in air using an Nd: YAG laser (DORNIER medTech Medilas 5100 fibertom, UK) beam, with 1064 nm wavelength, 40 W output power, power density about 3.258 KW/m^2, continues mode (CW), and combustion time 50 s. The laser beam was delivered by a single-mode fiber optic cable; with a length of 60 cm and a diameter of 125 μm; the distance between the sample and the fiber-optic cable end was 1 cm. Due to the small spot size of the laser beam, the combustion operation was performed point-by-point in an open air to obtain the ash. The laser was located on a holder, while the crucible was rotated every 50 s, carefully, for approximately 5 mm. This step was done again several times again for accuracy, before the investigations. The experimental work was carried out in the Institute of Laser, Sudan University of Science and Technology, Khartoum, Sudan. Only solid residues after laser combustion have been characterized in this work. Whereas gaseous products were also observed during laser combustion, they were not characterized. These gaseous products may be harmful to the environment; it is recommended to be characterized in future studies.

2.2 Characterization

The non-combusted and combusted palm fiber (sample 1 and sample 2, respectively) and non-combusted and combusted palm leaf (sample 3 and sample 4, respectively) were examined using X-Ray Diffractometer (XRD) (Shimadzu, MAX_X, XRD-7000, Japan), Cu K_α with a scanning speed of 1000°/min [13]. The data were collected for a two-theta (2θ) range of 10°–80° at a step size of 0.0002°. The samples were prepared by careful grinding, before the XRD measurements, using an agate mortar homogenization. XRD patterns were analyzed using the Materials Data, Inc., MDI Jade 0.5 Match Program. Chemical groups in the non-combusted and combusted samples were identified by a Fourier Transform InfraRed (FTIR) spectrometer (Satellite FTIR 5000, Japan). The samples were mixed with dry potassium bromide powder (KBr) at a ratio of 1:100. Through applying adequate pressure, the tablet was prepared for scanning. The FTIR spectra for the samples were collected, in the 400–3500 cm^{-1} wavenumber range, using an FTIR spectrometer.

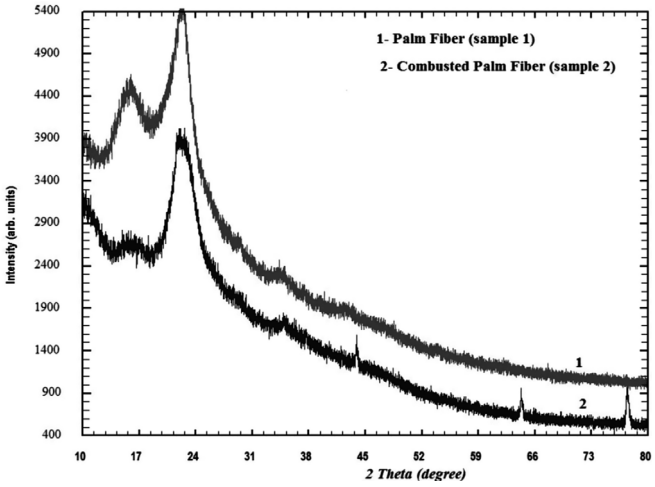

Fig. 1. XRD patterns of date-palm-fiber powder samples.

3 Results and discussion

3.1 XRD analysis

3.1.1 Palm fiber XRD

The XRD patterns of the palm fiber are depicted in Figure 1. The broad peak displayed here is attributed to an amorphous structure, and some of the other peaks indicate the crystalline species, as indicated in Table 1. The spectra of palm-fiber samples, before and after combustion analyzed by the Match Program are depicted in Figure 1. This figure confirms the existence of non-crystalline silica in the two samples, between 10° and 30° at a 2θ range of 21–23° (see Tables 1 and 2).

For the date-palm-tree fiber sample before combustion (sample 1, Fig. 1); carbon compounds such as acetamide (C_2H_5NO), dinite [NR] ($C_{20}H_{36}$), ikaite $CaCO_3H_2O$, hatrurite (Ca_3SiO_5) and $Ca_4Si_2O_6(CO_3)(OH)_2$, were observed. However, for date-palm-tree fiber sample after the combustion procedure (sample 2, Fig. 1), other new compounds including acetamide (C_2H_5NO), caoxite ($C_2H_6CaO_7$), caoxite ($C_2H_6CaO_7$), caoxite ($C_2H_6CaO_7$), portlandite (Ca$(OH)_2$), and graphite-2H(C), were observed. Notably, for sample 2, the combustion procedure using laser is highly effective in forming products, which appear in combusted samples such as portlandite ($Ca(OH)_2$), and graphite-2H (C) at 2θ values of 43.897°, 64.261°, 77.379°, and 77.525°, respectively (see Tables 1 and 2).

3.1.2 Palm leaves XRD

The XRD patterns of the date-palm leaves, before combustion (sample 3) and after combustion (sample 4) are shown in Figure 2 displaying the spectra of samples (3 and 4)

Table 1. Peak-search report of the palm-fiber, before combustion.

2-Theta	d (A°)	Height	I%	Area	I%	FWHM	Crystal structure with space group	Phase
15.460	5.7269	223	29.0	15309	23.5	0.834	Rhombohedral-single crystal, R3	Acetamide, syn C_2H_5NO (white)
15.970	5.5448	233	30.3	14416	22.1	0.752	Orthorhombic-P212121	Dinite [NR] $C_{20}H_{36}$ (colorless)
22.039	4.0299	599	77.9	47452	72.7	0.963	Orthorhombic-P212121	Dinite [NR] $C_{20}H_{36}$ (colorless)
22.180	4.0045	704	91.5	61147	93.7	1.056	Monoclinic-C2/c	Ikaite, syn $CaCO_3H_2O$ (colorless)
22.429	3.9607	769	100.0	65243	100.0	1.031	Rhombohedral-powder diffraction, R3m	Hatrurite, syn Ca_3SiO_5
22.727	3.9094	597	77.6	54163	83.0	1.103	Orthorhombic-powder diffraction	$Ca_4Si_2O_6(CO_3)(OH)_2$ (light brown, white)

Where: d is the spacing of the crystal planes, I is Intensity and FWHM is Full Width at Half Maximum.

Table 2. Peak-search report of the palm fiber, after combustion.

2-Theta	d (A°)	Height	I%	Area	I%	FWHM	Crystal structure with space group	Phase
21.746	4.0836	448	95.3	31711	81.7	0.860	Rhombohedral-single crystal, R3	Acetamide, syn C_2H_5NO (white)
21.971	4.0423	470	100.0	37315	96.2	0.965	Triclinic-powder diffraction	Caoxite, syn $C_2H_6CaO_7$
22.198	4.0014	389	82.8	38795	100.0	1.212	Orthorhombic-P212121	Dinite [NR] $C_{20}H_{36}$ (colorless)
22.503	3.9478	334	71.1	35197	90.7	1.281	Triclinic-powder diffraction	Caoxite, syn $C_2H_6CaO_7$
22.605	3.9301	291	61.9	26048	67.1	1.088	Triclinic-powder diffraction	Caoxite, syn $C_2H_6CaO_7$
64.261	1.4483	246	52.3	5691	14.7	0.281	Hexagonal-powder diffraction, P-3m1	Portlandite, syn $Ca(OH)_2$
77.379	1.2323	399	84.9	13333	34.4	0.406	Hexagonal-powder diffraction, P63/mmc	Graphite-2H(C) (black)
77.525	1.2303	272	57.9	12409	32.0	0.555	Hexagonal-powder diffraction, P-3m1	Portlandite, syn $Ca(OH)_2$

analyzed by the Match Program [3]. This confirms the existence of non-crystalline silica in all the samples in the broad peak range of $2\theta = 21° - 23°$ for the samples. However, some of the phases that did not appear in sample 3 were formed in sample 4, such as formicaite ($Ca(HCO_2)_2$), lonsdaleite (C) and cristobalite (SiO_2) at 2θ peaks of 37.555°, 43.799°, 64.169° and 77.296°, respectively (Fig. 2). Moreover, some phases that appeared in sample 3 spectrum disappeared in sample 4 which were moganite (SiO_2) and howlite ($C_6H_4(CO)_2C_6\ H_4$), at the 28.529° and 40.685° peaks, respectively (Fig. 2). The X-ray analyses of the palm leaves are presented in Tables 3 and 4. Phases that appeared in the sample 3 XRD spectrum but, disappeared in sample 4 this may be due to high temperature and high pressure from the focusing of laser photons through the combustion process.

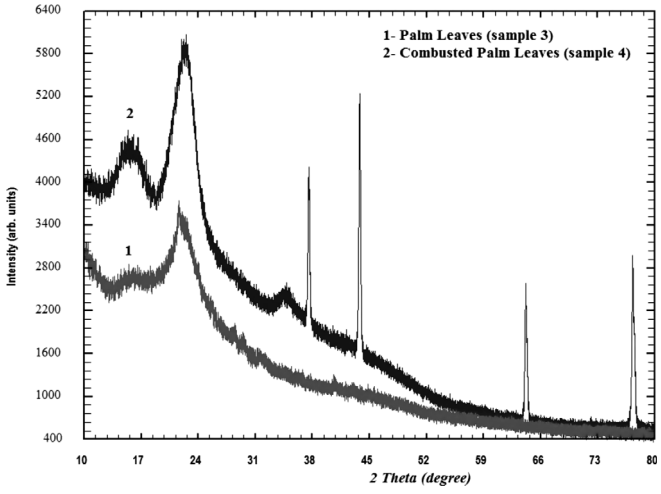

Fig. 2. XRD patterns of the palm-leaf powder samples.

3.2 FTIR studies/analysis

3.2.1 Palm-fiber FTIR analysis

The infrared spectrum reveals the entire molecular-structure information of the investigated samples. From the intensities and frequencies of some of the spectral bands, it is possible to predict the types of functional groups that exist in the molecules. The FTIR spectra for samples 1

Table 3. Peak-search report of the palm leaves, before combustion.

2-Theta	*d* (A°)	BG	Height	*I*%	Area	*I*%	FWHM	Crystal structure with space group	Phase
21.636	4.1041	3142	486	100.0	22667	74.2	0.567	Orthorhombic-single crystal, Cc	Hillebrandite $Ca_2(SiO_3)(OH)_2$
22.054	4.0272	3126	311	64.0	30568	100.0	1.195	Rhombohedral-single crystal, R3	Acetamide, C_2H_5NO (white)
22.376	3.9700	3113	249	51.2	28120	92.0	1.373	Monoclinic-powder diffraction, P21/n	Karpatite, $C_6H_2(C_4H_2)_4C_2H_2$ (red-violet)
28.529	3.1262	1755	140	28.8	3586	11.7	0.311	Monoclinic, I2/c	Morganite Si O_2
40.685	2.2158	1091	114	23.5	2970	9.7	0.317	Monoclinic-powder diffraction, P21/a	Howlite, $C_6H_4(CO)_2C_6H_4$

Table 4. Peak-search report of the palm leaves, after combustion.

2-Theta	*d* (A°)	BG	Height	*I*%	Area	*I*%	FWHM	Crystal structure with space group	Phase
21.998	4.0373	5231	521	16.4	47257	69.8	1.103	Triclinic-powder diffraction	Caoxite, $C_2H_6CaO_7$
22.179	4.0048	5192	646	20.4	57795	85.3	1.087	Monoclinic-(Unknown), P21 (4)	$C_{14}H_{10}$ (colorless, light gray, white)
22.457	3.9558	5110	738	23.3	66256	97.8	1.091	Rhombohedral-powder diffraction, R3m	Hatrurite, syn Ca_3SiO_5
22.623	3.9271	5084	718	22.6	60055	88.6	1.017	Triclinic-powder diffraction	Caoxite, syn $C_2H_6CaO_7$
37.555	2.3930	2016	2029	63.9	44222	65.3	0.265	Tetragonal-(Unknown), P41212	Formicaite $Ca(HCO_2)_2$ (light blue, white)
43.799	2.0652	1613	3174	100.0	67744	100.0	0.259	Hexagonal-powder diffraction, P63/mmc	Lonsdaleite, syn (C)
77.296	1.2334	565	2070	65.2	62866	92.8	0.369	Tetragonal-powder diffraction, P41212	Cristobalite, SiO_2 (colorless)

and 2 are depicted in Figure 3. The absorbance peak around 660, 420 cm^{-1} corresponds to the bending and stretching of the siloxane bonds (Si–O–Si) [3]. The peaks at approximately 1032 cm^{-1} in both samples, and at 1150 cm^{-1} in sample 2 (1260–700 cm^{-1}) indicate the possible stretching vibration for alkane C–C [14]. In general, the peaks at 1437 cm^{-1} appear because of the C–O stretching of carbonate [15]. Moreover, the absorbance band at the 1420 cm^{-1} peak indicates C–O vibrations or C–H deformation in the samples [16]. In general, the 1422 cm^{-1} peak appears because of the C–O stretching of carbonate [3]. The peak at 1650 cm^{-1} is indicated the aromatic stretching in palm-fiber structure and increases in sample 2 [17]. The weak band at 1506–1510 cm^{-1} is because of aromatic C–H. The absorbance peak around 2350 cm^{-1} is attributed to –C≡N– (Nitrites) and –C≡C– (Alkynes) compounds [16]. The peak in sample 1, around 2924 cm^{-1}, can be indicated the C–H stretching modes; the peak around 940 cm^{-1} is indicated to the asymmetric stretching of the CH_2 group.

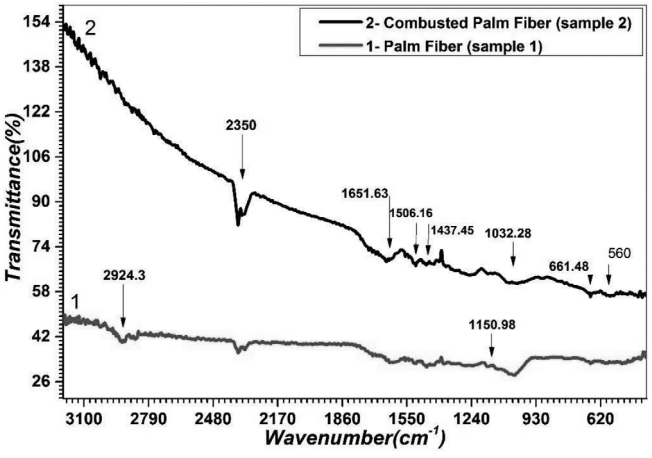

Fig. 3. FTIR results of non-combusted and combusted palm fiber.

3.2.2 Palm-leaf FTIR analysis

The FTIR spectra of the palm-leaves samples (samples 3 and 4) were investigated, revealing several graphene and silicon bonds (Fig. 4). The new absorbance peak around 2926–2843 cm^{-1} in sample 4, which did not exist in sample 3, can be indicated the C–H stretching modes. The absorbance peak around 2343 cm^{-1}, because of the –C≡N– (Nitrites) and –C≡C– (Alkynes) compounds [3, 14, 16], increases after combustion (sample 4). In addition, the

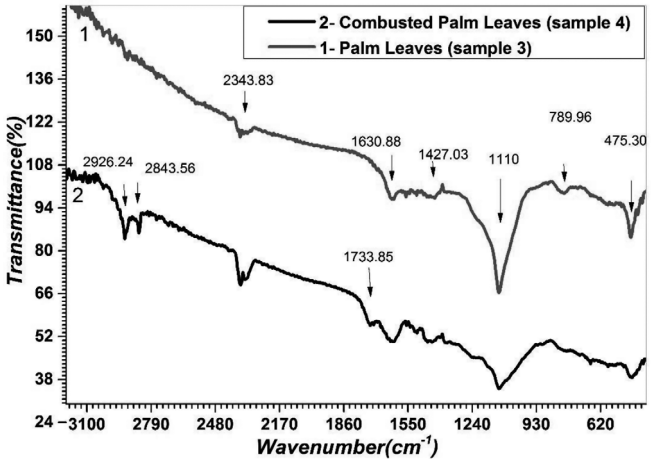

Fig. 4. FTIR results of non-combusted and combusted palm leaf.

additional peak formed in sample 4 at 1733 cm^{-1} maybe refers the carbonyl group (C=O) [17]. The strong peak at 1630 cm^{-1} is indicated the aromatic stretching in the palm-leaf structure, and decreases after the combustion process [18]. The absorbance band at the 1427 cm^{-1} peak may indicate C–O vibrations or C–H deformation in the samples [19]. In general, the 1422 cm^{-1} peak appears because of the C–O stretching of carbonate [20]. The strong absorbance peak at around 1110 cm^{-1} is indicated the Si–O–Si antisymmetric stretching mode, and the peaks from 790 to 470 cm^{-1} match siloxane bond (Si–O–Si) stretching and bending vibration [3, 14].

These results indicate that the laser heat has successfully modified the date-palm-tree residues samples by the interaction of laser photons with the molecules. When the high-power laser beam hits the agricultural waste, laser photons absorption and interaction occur. The main laser parameters that can be controlled during combustion include the wavelength, laser power, beam diameter, combustion time, and beam mode. In general, infrared wavelength produces a primarily thermal effect, but to obtain the highest productivity, high laser power is needed. So the power density of the laser is the most important parameter.

It was found, for example, that the combustion of one gram of agricultural waste could be completed in 50 s and 40 W by laser while 10 g required 1.5–10 min and 300–800 W power by microwave and at least 2 h with 1500 W power for conventional heating for 10 gramsminutes and 300–800 W power [21, 22]. Nd: YAG laser is equally effective but is less expensive in energy consumption than the oven for combustion, so it has both positive environmental and economic impacts. Although in recent years fiber lasers have become widespread and are gradually replacing solid-state lasers, Nd: YAG laser has more advantages in the combustion process; it is represented in that the fiber lasers are limited at output peak power of a few kilowatts where increasing the laser peak power leads to fiber damage due to nonlinear effects and high peak power at the output fiber. Despite semiconductor lasers having high-efficiency Nd: YAG Laser overtakes them with its high power.

In comparison, the conventional combustion using electrical heater it is difficult to control burning and furnace consumes more electrical power with more time of burning. Microwave also consumes more electrical power and it is not burning dry material easy and it takes more time and there is wave hazard around the microwave system. By using laser it saves the electrical power and the parameters (power, power density, combustion duration and wavelength) are under control as the results of XRD the crystalline structures of the products from the combustion may by be changed using different power and different combustion duration.

Basically; laser sources have a very small waist; this caused difficulty in combusting and gives a small amount of production. It is expected that using beam expander to increase the expansion of the combustion area and increase the output power will increase the efficiency of combustion. Additional optimization opportunities exist in making the sample move in a production line (moving belt) with a fixed laser source, which would allow the products of combustion in a reasonable amount. Several researchers have done significant investigations on the treating of a great amount of material with laser and the influence of laser parameters. In some set-ups, material move either on a special conveying belt with a constant speed over an area illuminated by a laser beam [23] or by the free-falling method [24]. In another method, a rotating laser beam sweep is installed [25]. Some researchers used a set-up containing many lasers [26, 27]. In addition, to provide the optimum laser parameters (beam spot size, optical power densities, intensity, etc) optics such as lenses beam expander were used [28–30], as well as the passing velocity and distance between laser and material can be also adjusted.

In future, the transformation of a large amount of agricultural wastes using laser-induced combustion; can be an economically method to obtain raw material to produce a lot of useful and high-value materials.

4 Conclusions

In summary, date-palm-tree fibers and leaves were combusted, using an Nd: YAG laser (1064 nm) with 40 W output power for 50 s. Two different procedures were utilized to identify the crystal structure and functional groups of the date-palm-tree fibers and leaves and their products after combustion. The first was XRD, which utilized to investigate the crystal structure. The XRD patterns of the combusted date-palm-tree fibers and leaves reveal the presence of crystalline materials such as portlandite ($Ca(OH)_2$), and graphite-2H(C). The second method was FTIR, which utilized to investigate the chemical groups of the four samples. It was found that the palm-fiber samples contained siloxane, aromatic, nitrites, and alkynes. In contrast, the palm-leaf samples contained graphene, silicon, nitrites, alkynes, carbonyl, siloxane, and aromatics. The gaseous products of this combustion method, apart from CO_2 (GHG), may be harmful to the environment; it is recommended to investigate them in future research. The present study provides a foundation for future research to apply

laser technology in waste treatment to contribute to a better environment.

Acknowledgments. The authors are grateful to the Institute of Laser, Sudan University of Science and Technology, Khartoum, Sudan, for conducting this work.

References

1 Almi K., Lakel S., Benchabane A., Kriker A. (2015) Characterization of date palm wood used as composites reinforcement, *Acta Phys. Pol. A* **127**, 1072.

2 Sadh P.K., Duhan S., Duhan J.S. (2018) Agro-industrial wastes and their utilization using solid state fermentation: a review, *Bioresour. Bioprocess.* **5**, 1, 1–15.

3 Gawbah M.A.P., Marouf A.A., Alsabah Y.A., Orsod M.U., Elbadawi A.A. (2018) Synthesis of silica, silicon carbide and carbon from wheat bran and converting its crystal structure using Nd: YAG laser, *Int. J. Adv. Res. Phys. Sci.* **4**, 11, 31.

4 Gawbah M.A.P., Elbadawi A.A., Alsabah Y.A., Orsod M.U., Marouf A.A. (2018) Characterization of the crystal structure of sesame seed cake burned by Nd: YAG laser, *J. Mater. Sci. Chem. Eng.* **6**, 4, 121.

5 Pode R. (2016) Potential applications of rice husk ash waste from rice husk biomass power plant, *Renew. Sustain. Energy Rev.* **53**, 1468–1485.

6 Chaib H., Kriker A., Mekhermeche A. (2015) Thermal study of earth bricks reinforced by date palm fibers, *Energy Procedia* **74**, 919–925.

7 Hosseinkhani H., Euring M., Kharazipour A. (2015) Utilization of date palm (*Phoenix dactylifera* L.) pruning residues as raw material for MDF manufacturing, *J. Mater. Sci. Res.* **4**, 1, 46.

8 Bolshov M.A., Kuritsyn Y.A., Romanovskii Y.V. (2015) Tunable diode laser spectroscopy as a technique for combustion diagnostics, *Spectrochim. Acta B: At. Spectrosc.* **106**, 45–66.

9 Puli A., Kumar J.J. (2016) Laser Ignition System for IC Engines, *Int. J. Sci. Res. Sci. Eng.* **2**, 5, 76–79.

10 Merico E., Grasso F.M., Cesari D., Decesari S., Belosi F., Manarini F., de Nuntiis P., Rinaldi M., Gambaro A., Morabito E., Contini D. (2020) Characterisation of atmospheric pollution near an industrial site with a biogas production and combustion plant in southern Italy, *Sci. Total Environ.* **717**, 137220.

11 Liu J. (2016) High pressure x-ray diffraction techniques with synchrotron radiation, *Chin. Phys. B* **25**, 7, 076106.

12 Wangler T., Roussel N., Bos F.P., Salet T.A., Flatt R.J. (2019) Digital concrete: a review, *Cem. Concr. Res.* **123**, 105780.

13 Ali B.M., Siddig M.A., Alsabah Y.A., Elbadawi A.A., Ahmed A.I. (2018) Effect of Cu^{2+} doping on structural and optical properties of synthetic $Zn_{0.5}Cu_xMg_{0.5-x}Fe_2O_4$ (x = 0.0, 0.1, 0.2, 0.3, 0.4) nano-ferrites, *Adv. Nano Res.* **7**, 1, 1.

14 Martínez-Casillas D.C., Vázquez-Huerta G., Pérez-Robles J. F., Solorza-Feria O. (2011) Electrocatalytic reduction of dioxygen on PdCu for polymer electrolyte membrane fuel cells, *J. Power Sources.* **196**, 10, 4468–4474.

15 Mironov E., Koretz A., Petrov E. (2002) The research of detonation Nanodiamond structure by optical methods, *Diam. Relat. Mater.* **11**, 872–876.

16 Akemi Ooka A., Garrell R.L. (2000) Surface-enhanced Raman spectroscopy of DOPA-containing peptides related to adhesive protein of marine mussel, Mytilus edulis, *Biopolymers* **57**, 2, 92–102.

17 Tobin M.C., Carrano M.J. (1956) Infrared spectra of polymers. I. Effect of crystallinity on the infrared spectrum of polyethylene and on the infrared spectra of Nylon 6 and Nylon 11, *J. Chem. Phys.* **25**, 5, 1044–1052.

18 Chefetz B., Hatcher P.G., Hadar Y., Chen Y. (1996) Chemical and biological characterization of organic matter during composting of municipal solid waste, *J. Environ. Qual.* **25**, 4, 776–785.

19 Susi H., Byler D.M. (1983) Protein structure by Fourier transform infrared spectroscopy: second derivative spectra, *Biochem. Biophys. Res. Commun.* **115**, 1, 391–397.

20 Madhu P., Sanjay M.R., Senthamaraikannan P., Pradeep S., Saravanakumar S.S., Yogesha B. (2019) A review on synthesis and characterization of commercially available natural fibers: part II, *J. Nat. Fibers* **16**, 1, 25–36.

21 Rungrodnimitchai S., Phokhanusai W., Sungkhaho N. (2009) Preparation of silica gel from rice husk ash using microwave heating, *J. Met. Mater. Miner.* **19**, 2, 45–50.

22 Rungrodnimitchai S. (2010) Modification of rice straw for heavy metal ion adsorbents by microwave heating, *Macromol. Symp.* **295**, 1, 100–106.

23 Muszyñski S., Gladyszewska B. (2008) Representation of He–Ne laser irradiation effect on radish seeds with selected germination indices, *Int. Agrophys.* **22**, 1, 151–157.

24 Ri P., Choe S., Jang Y. (2019) Study on laser pre-sowing treatment of rice seeds by free-falling transport method, *Inf. Process. Agric.* **6**, 4, 515–521.

25 Sevostyanova N.N., Pchelina E.A., Gordievskaia V.O., Danilovskikh M.G., Trezorova O.Y. (2020) Effect of laser irradiation on the processes involved in growth of mustard and radish seeds, in: *IOP Conference Series: Earth and Environmental Science*, vol. **613**, IOP Publishing, p. 012136.

26 Hasan M., Hanafiah M.M., Aeyad Taha Z., Alhilfy I.H., Said M.N.M. (2020) Laser irradiation effects at different wavelengths on phenology and yield components of pretreated maize seed, *Appl. Sci.* **10**, 3, 1189.

27 Yuri S., Jarbas C. (2021) Effects of 660 nm laser irradiation of soybean seeds on germination, emergence and seedling growth, *Acta Agrophys.* **28**, 5–18.

28 Janayon R.V.B., Guerrero R.A. (2019) Laser irradiation of mung bean (*Vigna radiata* L.) at two wavelengths for enhanced seedling development, *Int. J. Opt.*, **2019**, 1–7.

29 Hasan M., Hanafiah M.M., Taha Zaeyad A.I., Said M.N.M. (2020) Effect of low-intensity laser irradiation on field performance of maize (*Zea mays* L.) emergence, phenological and seed quality characteristics, *Appl. Ecol. Environ. Res.* **18**, 4, 6009–6023.

30 Jevtić S.D., Srećković M.Ž., Pelemiš S.S., Konstantinović L. M., Jovanić P.B., Petrović L.D., Dukić M.M. (2015) Laser influence to biosystems, *Hem. Ind.* **69**, 4, 433–441.